Advances in Engineering Software 42 (2011) 94–107

Contents lists available at ScienceDirect

Advances in Engineering Software

journal homepage: www.elsevier.com/locate/advengsoft

A versatile software tool making best use of sparse data for closed loop process control

Mehmet Önder Efe

Department of Electrical and Electronics Engineering, Bahçeşehir University, Beşiktaş, İstanbul 34349, Turkey

ARTICLE INFO

Article history:
Received 23 July 2010
Received in revised form 4 November 2010
Accepted 18 December 2010
Available online 14 January 2011

Keywords:
Bioreactor benchmark problem
Sliding mode control
Process control
Support Vector Machine
Learning with few data
Cell mass control

ABSTRACT

This paper presents the design of a software supported sliding mode controller for a biochemical process. The state of the process is characterized by cell mass and nutrient amount. The controller is designed for tracking of a desired profile in cell mass and it is shown that the nutrient amount in the controlled bioreactor evolves bounded. A smart software tool named Support Vector Machine (SVM), which minimizes the upper bound of an empirical risk function, is proposed to approximate the nonlinear function seen in the control law by using very limited number of numerical data. This removes the necessity of knowing the functional form of the nominal nonlinearity in the control law. It is shown that the controller is robust against noisy measurements, considerable amount of parameter variations, discontinuities in the command signal and large initial errors. The contribution of the present work is the achievement of robustness and tracking performance on a benchmarking process, under the presence of limited prior knowledge.

1. Introduction

Chemical processes often display a complicated behavior due to the strong interdependencies between the variables involved. Although in some cases the process is described by a few state variables, obtaining good disturbance rejection with high tracking precision requires implementing nonlinear control laws. The performance obtained with nonlinear control laws cannot be achieved in general by utilizing the their counterparts designed through the use of linearized or simplified models of the process. This aspect of chemical processes make them good test beds for benchmarking. A review of nonlinear control techniques on chemical processes is presented in [4], where the feasibility and efficacy of nonlinear control laws are discussed with an emphasis on relevant control challenges displayed by chemical processes.

Ungar [32] defines a bioreactor benchmark problem that excellently fits in the context. The state of the process is described by two variables named the cell mass denoted by $c_1(t)$ and the amount of nutrients denoted by $c_2(t)$ (see [32,25,12]). The reaction tank is assumed to be unity volume and the dimension for the cell mass and the nutrients is grams per volume, i.e. the concentration of the relevant variable. The goal is to maintain the cell mass at desired levels by altering the inflow rate at a rate equal to outflow rate keeping the reaction volume constant. The challenges associated with the control of the bioreactor process are the nonlinearity enabling the emergence of a rich set of dynamical regimes, instabilities caused even by tiny variations in the process variables and the presence of a long control sampling interval in the feedback loop. These difficulties constitute a solid motivation to design a software support to a feedback control mechanism.

In the past, bioreactor benchmark problem was studied several times for feedback control purposes. In [12], this problem is considered for developing a nonlinear control law forcing the process states to those of a first order linear one. Feedforward neural networks are used to build the nonlinear function in the control law and the plant is forced to follow a reference model. Puskorius and Feldkamp study this problem in the context of demonstrating the efficacy of a neural network learning algorithm and consider the control problem about a setpoint in the stable region, another setpoint in the unstable region and a transition between these regions [25]. The controller proposed in our study forces the system toward the stable region as will be discussed in the sequel. Brengel and Seider propose a multi step nonlinear controller based on predictive control theory and validate the performance of the closed loop control system on a variant of the model considered here. The authors emphasize the preferability of operating at highest possible cell mass solutions, which are desired to be reasonably away from the region of periodic oscillations [5]. Anderson and Miller [1] emphasize that the controller design for the bioreactor benchmark problem addressed here is a challenge due to the nonlinearity and the a set of complicated regimes that arise due to it. Clearly, the works mentioned above motivate us to position the merit and effectiveness of sliding mode control techniques in the

E-mail address: onderefe@gmail.com

0965-9978/$ - see front matter © 2010 Elsevier Ltd. All rights reserved.
doi:10.1016/j.advengsoft.2010.12.006

control of continuously stirred tank reactors. In this paper, we consider the problem of trajectory tracking in the cell mass and we analyze the limitations of the design carried out with a thorough discussion.

Sliding Mode Control (SMC), also known as Variable Structure Control, is a well established approach ensuring some degrees of robustness against uncertainties in the feedback loop. The underlying idea is to create a sliding subspace, which is an attractor due to the philosophy of the design [16,33]. SMC technique, which has many successful applications in motion control systems, is also applied for feedback control of chemical processes. See for example [15], where the process is modeled by a partial differential equation [6], where the design is based on a first order model including dead time, and [9], where a second order sliding mode control is performed after feedback linearization. One fact in all these studies needs emphasis: The sliding mode controller drives the system toward the sliding manifold and maintains the evolution on that loci, which is stable by the design and the error converges the origin of the phase space. Once the trajectories are confined to the sliding manifold, the control system displays some degrees of robustness against disturbances and parameter variations in system dynamics. This response is called invariance property of sliding mode control [20,16,7,19]. The underlying idea in this paper is to implement a robust controller for the bioreactor benchmark problem. The reaching law approach in [16] is followed and it is assumed that limited number of numerical data are available about the nominal plant nonlinearities. This information is used in the training of a support vector machine, which is introduced in the pioneering work of Vapnik for classification and regression problems [34]. This new approach aims at minimizing a structural risk, i.e. the upper bound of an appropriately defined generalization error. Not only because of this fact SVMs are superior to conventional neural networks, but also the lack of multiple local minima in SVM learning and the lack of best configuration search effort make SVMs attractive to use instead of conventional neural network structures, the training algorithms of which minimize the empirical risk over a set of training pairs instead of its bound (see [13,10]). The very role of the SVM in the problem studied here is to demonstrate that the dependence of the control law to the nominal plant nonlinearities can even be loosened by utilizing a limited number of numerical data without giving concessions from stability and accuracy. This aspect of the proposed strategy makes it more practicable than those requiring exact form of the nonlinear expressions. Despite the application fields of SVMs cover a broad spectrum [14,22,3], the realm of control engineering is a prime area that has benefited from the possibilities offered by this versatile software tool. In the research reported by [17], SVMs are applied for the water level control in a three tank system. Combination of SVMs with neuro fuzzy systems is presented by [18], use of SVMs in the context of model predictive control is elaborated by [26,27,2]. An application exploiting SVM tool in the field of optimal control is considered by [23] and the use of least squares type SVMs is elaborated by [29]. The use of SVMs with Cerebellar Model Articulation Controller (CMAC) is reported by [8], with internal model control is reported by [36], and with adaptive inverse control is reported by [35]. Recent works focusing on SVM aided sliding mode control report the chattering elimination issue in [24], output feedback notion in [31] and time varying sliding surface design in [30]. These works and the recent trend in the use of SVMs in control systems constitute a strong motivation for us to develop software tools facilitating the closed loop control tasks in process engineering.

This paper is organized as follows. Section 2 introduces the bioreactor benchmark problem and analyzes its behavior. Section 3 defines the semi sliding mode control problem and emphasizes the main result of this work. The design of the nonlinear feedback controller is presented in Section 4, and SVM based estimator utilized in this paper is summarized in Section 5. Section 6 is devoted to the operating conditions, simulation results and their interpretations. The concluding remarks are given at the end of the paper.

2. Bioreactor benchmark problem

The bioreactor is a tank in which the biological cells are mixed with nutrients and water as shown in Fig. 1. The cells and nutrients are in a dynamical interaction modeled by Eqs. (1) and (2), where $c_1(t)$ denotes the cell mass while $c_2(t)$ stands for the nutrient amount. The process is continuously fed by pure water and the variable characterizing the inflow rate is denoted by $w(t)$. In order to maintain the reaction volume constant, the contents of the tank is removed at a rate equal to the inflow rate, $z(t)$, which is composed of a mixture of cells, nutrients and water. The goal of the control problem is to achieve the tracking of a desired temporal evolution in cell mass. The state variables of the process and limited numerical information about the nonlinearities seen below are assumed to be available for constructing the controller.

$$\dot{c}_1(t) = -c_1(t)w(t) + c_1(t)(1 - c_2(t))e^{\frac{c_2(t)}{\gamma}} \tag{1}$$

$$\dot{c}_2(t) = -c_2(t)w(t) + c_1(t)(1 - c_2(t))e^{\frac{c_2(t)}{\gamma}}\frac{1+\beta}{1+\beta-c_2(t)} \tag{2}$$

where the state variables are constrained by $\Omega := \{0 \leqslant c_1(t), c_2(t) \leqslant 1\}$. In the nominal plant model given above, the growth rate is characterized by the parameter $\beta = 0.02$ and the nutrient inhibition parameter is given by $\gamma = 0.48$.

In Fig. 2, several trajectories are shown for a set of initial conditions denoted by a circle. Each subplot depicts the evolution of the system at a constant inflow rate indicated on the top. Depending on the value of the inflow rate, the attractors change their locations and new attractors emerge as well. One visible one is a limit cycle which becomes apparent when $w = 0.75$. When $w = 0.8290$, the system changes its qualitative behavior radically. Computing the equilibrium values corresponding to this inflow rate, one obtains $c_1 = 0.1331$ and $c_2 = 0.8626$. The eigenvalues of the linearized system of equations at this point stipulate that in the increasing direction of c_2, the system undergoes Hopf bifurcation at this operating point and turns into an unstable one displaying spontaneous oscillations due to the limit cycle. In this regime, cell mass varies in between 0.1219 and 0.1466 while the nutrient amount fluctuates in between 0.8243 and 0.8996. At the points of crossing the imaginary axis, the eigenvalues of the linearized model are approximately equal to $0 \pm j1.7543$, from which we infer that the self sustained oscillations are quite fast.

In Fig. 3, the limit cycle and the convergence of the neighboring trajectories are illustrated for $w = 1.2$. In fact, limit cycles can occur for all values of admissible inflow rates, i.e. $0 \leqslant w \leqslant 2$. According to Bendixson theorem (see [28,21]), since the quantity

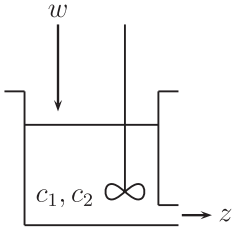

Fig. 1. Reaction tank with equal inflow and outflow rates.

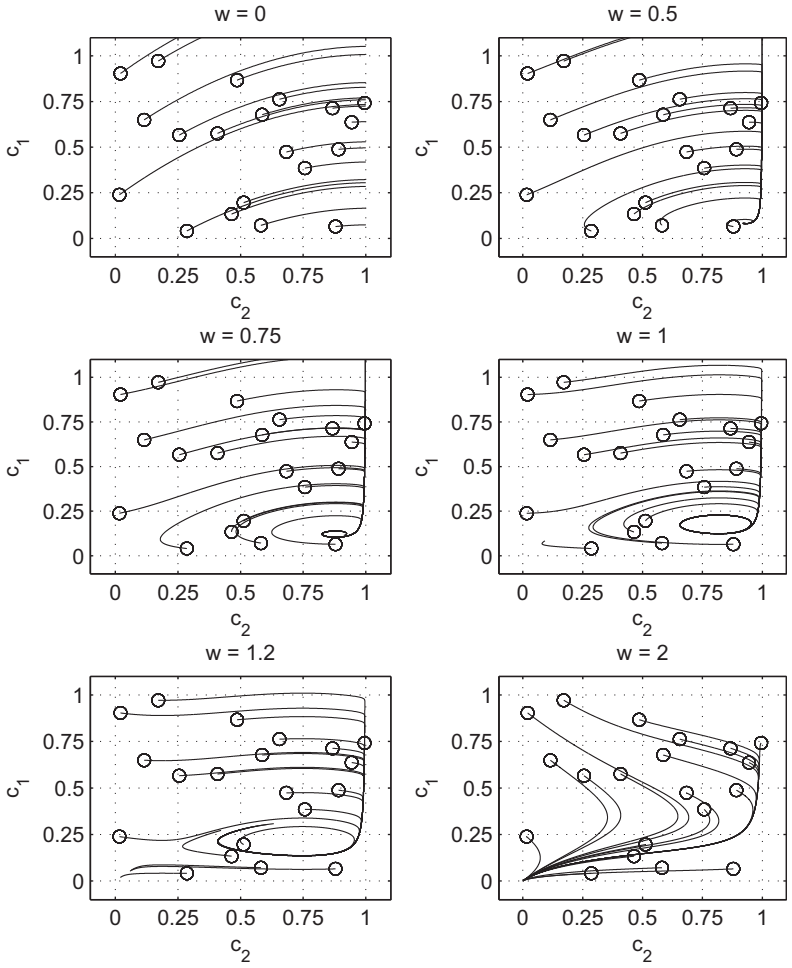

Fig. 2. The evolution of the process state for different initial conditions and at different inflow rates. The trajectories are for 20 s time.

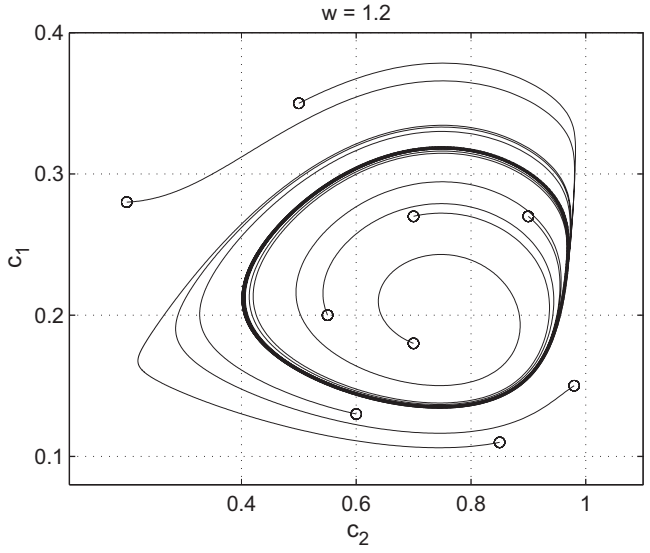

Fig. 3. Limit cycle arising when $w = 1.2$

$$H := \frac{\partial}{\partial c_1}\left(-c_1 w + c_1(1-c_2)e^{\frac{c_2}{\gamma}}\right) + \frac{\partial}{\partial c_2}\left(-c_2 w + c_1(1-c_2)e^{\frac{c_2}{\gamma}}\frac{1+\beta}{1+\beta-c_2}\right) = -2w + h(c_1,c_2) \tag{3}$$

does not vanish and does not change sign in $\Lambda \subseteq \Omega$, no limit cycles can exist entirely in Λ. For a given constant w, the curve of sign change for H is moved to the curve described by $h(c_1, c_2) = 2w$. Therefore one should run the quantity $2w$ from 0 to 4 and determine where the sign change occurs. In Fig. 4, the regions where the limit cycles cannot lie entirely within are depicted as white regions, termed Λ above, and the value of $2w$ is contoured for $2w$ equals to 0,2,3 and 4. According to this result, we figure out that it is possible to have other limit cycle trajectories in the system dynamics and Λ is a significantly wide subspace of Ω. From the control engineering point of view, this practically tells us that during the controlled operation of the process, many attractors and/or repellers can be created or destroyed depending on the value of w and the controller must be overcoming the dynamical influence of such difficulties while meeting the performance specifications and revealing disturbance rejection.

Consider the process at the steady state, i.e. $\dot{c}_1 = 0$ and $\dot{c}_2 = 0$. This yields the steady state control action $w_{ss} = (1-c_2)e^{\frac{c_2}{\gamma}}$ and with this control signal $\dot{c}_2 = (1-c_2)e^{\frac{c_2}{\gamma}}(-c_2 + c_1 g)$, i.e. when the steady state is reached c_2 is either 1 or a value that satisfies $g = c_2/c_1$ where $g(c_2(t)) := \frac{1+\beta}{1+\beta-c_2(t)}$. In the top subplot of Fig. 5, the parabolic (lower) curve depicts the solution obtained from $-c_2 + c_1 g = 0$. The same subplot also depicts the value of steady state control action w_{ss}. This figure stipulates that when the steady state is reached, the cell mass cannot assume values larger than $\frac{1+\beta}{4} = 0.255$. This practical constraint was also highlighted in [25] and [12]. The bottom subplot of Fig. 5 depicts how an arbitrary value of $(c_1(t_0),\ c_2(t_0))$ moves under the control action w_{ss}. Few

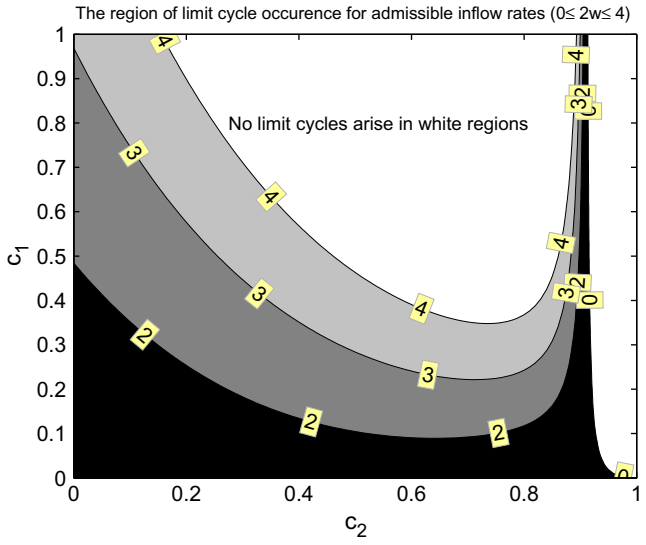

Fig. 4. Regions where limit cycles cannot occur are designated by white color.

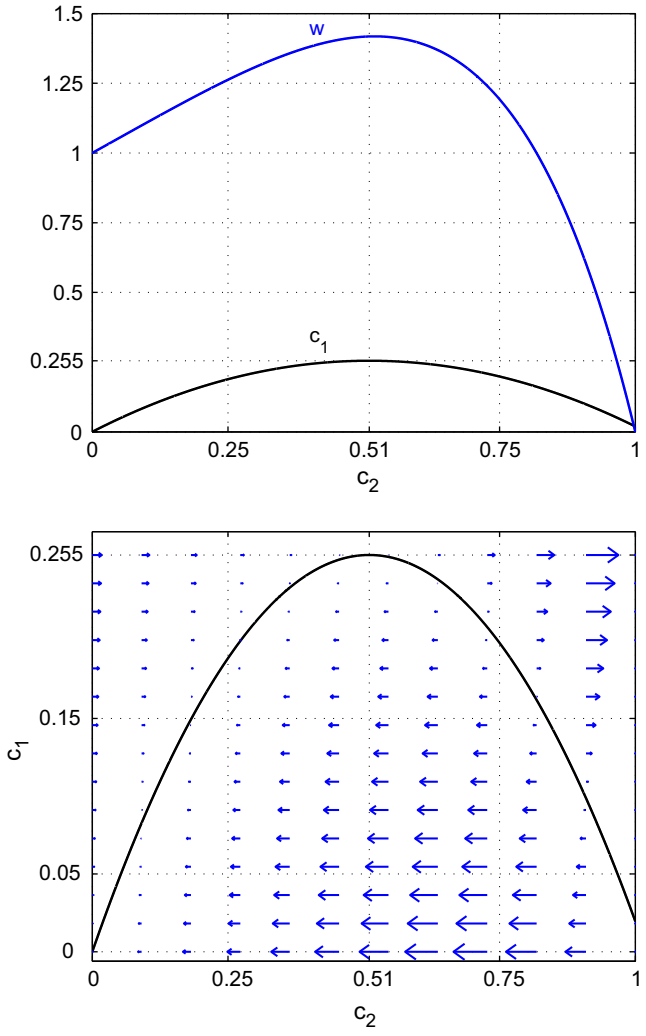

Fig. 5. Equilibrium points and the behavior with steady state control signal w_{ss}.

comments can be made for the motion for $t > t_0$ with w_{ss}. If $c_1(t_0) > \frac{1+\beta}{4}$ then the final value of the state vector is $(c_1(\infty), c_2(\infty)) = (c_1(t_0), 1)$. If $c_1(t_0) < \frac{1+\beta}{4}$, then any initial condition that is below the curve defined by $-c_2 + c_1 g = 0$ moves in the horizontal direction and stops on the left segment of the curve $-c_2 + c_1 g = 0$, which is shown in the bottom subplot of Fig. 5. Alternatively, the initial conditions that are above the curve defined by $-c_2 + c_1 g = 0$ move right until an equilibrium is reached, i.e. those satisfying $c_2(t_0) < \frac{1+\beta}{2}$ converge the left segment of the curve $-c_2 + c_1 g = 0$, however those with $c_2(t_0) > \frac{1+\beta}{2}$ stop at $(c_1(\infty), c_2(\infty)) = (c_1(t_0), 1)$. At the point $(c_1(t_0), c_2(t_0)) = (\frac{1+\beta}{4}, \frac{1+\beta}{2})$, the eigenvalues of the linearized system are both equal to zero. According to the behavior indicated by the vector field (flow), we conclude that this point is a half stable point, i.e. the trajectories close to this point but below $-c_2 + c_1 g = 0$ behave different from those above $-c_2 + c_1 g = 0$. This discussion with the flow illustrated in Fig. 5 clarifies the stability of the equilibrium states thoroughly.

A last point that should be emphasized is the effect of sampling in the control loop. In [32], the equation system in (1) is discretized by Euler method and a step size $\Delta = 0.01$ s is used. The sampling period for the control signal, called macro time steps ([25]) is equal to 50 Δs, which is long enough for the bioreactor process to develop deviations and spontaneous oscillations from a desired setpoint or a trajectory. In this paper, we test the performance of the proposed controller by operating it at the same rates too.

In [32], Ungar points out that although this system is not a completely realistic model of any bioreactor, which may display totally different time scales other than seconds, as seen from the presented discussion, the system considered in this paper displays several challenges highlighted also by [1] with a similar motivation. Due to the presented properties of the system, the model constitutes a good candidate for scrutinizing the merits and effectiveness of nonlinear control laws exploiting the possibilities offered by versatile software tools.

3. Main result

Definition 1. The semi sliding mode control problem is to force the state vector of a dynamical process to a subspace of the state space where some states are constrained to follow a predefined set of reference signals while the remaining ones are constrained to evolve bounded.

Clearly, the above definition of the control problem requires a very careful study of stability issues. Under such a problem setting, one can design a controller and check (i) whether the states under tracking penalty follow the reference signals via conventional Lyapunov analysis, and (ii) whether the remaining states evolve bounded under the designed feedback control strategy. Following theorem describes the chosen form of the control law.

Theorem 3.1. *Let $r(t)$ be a differentiable desired profile for the cell mass $c_1(t)$, and let $e_1(t) := r(t) - c_1(t)$ be the error in cell mass. Let $s(t) = e_1(t)$ be the switching function and define the sliding subspace (sliding manifold) by $(s, c_2) \in 0 \times (0, 1)$. If the nominal plant nonlinearity is denoted by*

$$f(c_1(t), c_2(t)) := c_1(t)(1 - c_2(t))e^{\frac{c_2(t)}{\gamma}}$$

then with $\zeta, \eta > 0$, the sliding mode control law given by

$$w(t) = \frac{-\dot{r}(t) + f(c_1, c_2) - \zeta \mathrm{sgn}(s(t)) - \eta s(t)}{c_1(t)} \tag{4}$$

ensures hitting in finite time and $(s, c_2) \in 0 \times [0, 1]$ is forced.

Note that parallel to the closed loop control goal, the phase space is $(s, c_2) \in \Re \times [0, 1]$ and the sliding subspace is a line segment characterized by $s = 0$ and $c_2 \in (0, 1)$. It should further be noted that the law in (4) needs the function f, however, in the

sequel, the function will be replaced by a SVM based predictor exploiting limited number of data and outputting $\hat{f}$. The proof of the above theorem is given in the next section.

4. Semi sliding mode control of the bioreactor

In this section, the claims in Theorem 3.1 are justified with analytical details. The design presented is based on the nominal representation seen in (1) and (2).

First, choose the Lyapunov function candidate

$$V = \frac{1}{2}s^2 \tag{5}$$

which clearly does not contain any information about the boundedness of c_2. The time derivative of the Lyapunov function in (5) is given by $\dot{V} = \dot{s}s$. For a $\zeta > 0$, if a control law assures

$$\dot{s}s \leqslant -\zeta|s| \tag{6}$$

then all trajectories are forced towards the locus described by $s = 0$ in the phase space. Equivalently, choosing the reaching law approach (see [16]) and setting a reaching dynamics as below ensures the hold of (6);

$$\dot{s} = -\zeta\ \mathrm{sgn}(s) \tag{7}$$

which can further be modified as

$$\dot{s} = -\zeta\ \mathrm{sgn}(s) - \eta s \tag{8}$$

to speed up the reaching as $\eta > 0$ and $\dot{s}s = -\zeta|s| - \eta s^2$ is forced. The hitting in finite time can be shown as below. Note that when hitting occurs, $s(t_h) = 0$ and $\dot{s}(t_h) = 0$ are satisfied. Here, t_h denotes the hitting time, i.e. the time elapses till a nonzero value of $s(0)$ reaches the sliding subspace.

$$s(t_h) = s(0) - \int_0^{t_h} (\zeta\ \mathrm{sgn}(s(\tau)) + \eta s(\tau))\mathrm{d}\tau \tag{9}$$

The quantity $\mathrm{sgn}(s(t))$ is constant and does not change sign until the time of hitting. Therefore we have

$$s(t_h) = s(0) - \mathrm{sgn}(s(0)) \int_0^{t_h} (\zeta + \eta\ |s(\tau)|)\mathrm{d}\tau = 0 \tag{10}$$

Or alternatively

$$\mathrm{sgn}(s(0))\left(|s(0)| - \int_0^{t_h} (\zeta + \eta\ |s(\tau)|)\mathrm{d}\tau\right) = 0 \tag{11}$$

Paraphrasing and rearranging (11) yields

$$|s(0)| = \int_0^{t_h} (\zeta + \eta\ |s(\tau)|)\mathrm{d}\tau \geqslant \int_0^{t_h} \zeta\ \mathrm{d}\tau = \zeta\ t_h \tag{12}$$

The hitting time t_h satisfies $t_h \leqslant \frac{|s(0)|}{\zeta}$, which puts a finite upper bound on the time interval for reaching the sliding subspace, i.e. $e_1(t) = 0$ is reached in finite time. Once the system is in the sliding mode, the motion is confined to the sliding subspace thereafter. This result guarantees that the desired cell mass profile is followed. For a detailed discussion on SMC technique, one should refer to [33,28,38].

If the phase space is $\Re^n$ then the sliding motion takes place in $\Re^{n-1}$. Clearly as in the case we present here, for $n = 1$ the sliding mode control problem reduces to the reaching mode as the sliding subspace is zero dimensional. It is still possible to interpret the approach within the context of sliding mode control as it displays the robustness against uncertainties and invariance properties, all subject to the same mathematical treatment.

According to the above discussion, and the chosen Lyapunov function, one sees that the control law in (4) ensures $(s, c_2) \to (0, \Re)$, i.e. the cell mass follows a desired profile, but this is clearly insufficient as the nutrient amount is desired to satisfy $0 < c_2 < 1$. Remember $g(c_2(t)) = \frac{1+\beta}{1+\beta-c_2(t)}$, drop the arguments of the variables for simplicity and solve the variable w from (1) and substitute into (2). This yields

$$\dot{c}_2 = \left(g - \frac{c_2}{c_1}\right)f + \frac{c_2}{c_1}\dot{c}_1 \tag{13}$$

Note the equality in (13) is satisfied regardless of the selected inflow rate (w). Rearranging (13), we obtain the expression below, and the solution in (15)

$$\int_0^t \left(\frac{\dot{c}_2}{c_2} - \frac{\dot{c}_1}{c_1}\right)\mathrm{d}\tau = \int_0^t \left(g - \frac{c_2}{c_1}\right)\frac{1}{c_2}f\,\mathrm{d}\tau \tag{14}$$

$$c_2(t) = \frac{c_2(0)}{c_1(0)}c_1(t)e^{I(t)} \tag{15}$$

where

$$I(t) = \int_0^t \left(g - \frac{c_2}{c_1}\right)\frac{f}{c_2}\mathrm{d}\tau \tag{16}$$

The evolution of $c_2(t)$ should be analyzed for two cases, namely $\dot{r} = 0$ case, where the reference signal is a constant, and $\dot{r} \neq 0$ case, where the reference signal is changing.

4.1. The First Case, $\dot{r} = 0$

We analyze the steady state conditions with three lemmas given below.

Lemma 4.1. *If for some t_1, $c_1(t_1) = 0$, then at $t = t_1$*

$$\dot{c}_1 = 0 \tag{17}$$

$$\dot{c}_2 = -c_2 w \tag{18}$$

which require $w = 0$ for arriving at a steady state for $t \geqslant t_1$.

Clearly from (17) and (18), the system arrives at the steady state when $w = 0$. Alternatively, any nonzero control action for $t > t_1$ to recover this forces $c_2(t) \to 0$ and the steady state described by $c_1 = c_2 = 0$ is reached as $t \to \infty$. Once the system is at $c_1 = c_2 = 0$, then the control action is functionless. Therefore $c_1(t) = 0$ is highly undesirable. Physically, $c_1 = c_2 = 0$ means that there are no cells in the reactor tank and no nutrients to feed the cells.

Lemma 4.2. *If for some t_2,$c_2(t_2) = 1$, then at $t = t_2$, we have the system of equations*

$$\dot{c}_1 = -c_1 w \tag{19}$$

$$\dot{c}_2 = -w \tag{20}$$

which require $w = 0$ for arriving at a steady state for $t \geqslant t_2$.

Due to Lemma 4.2, maintaining $c_2(t) = 1$ for $t \geqslant t_2$ requires $w = 0$, which stops the change in c_1 and the system is trivially in the steady state. Any nonzero control action to reduce c_2 causes a reduction in c_1 and this may trigger the results that arise when $c_1(t) = 0$. Physically, the nutrient amount is at its highest value and the cells within the tank are overfed. Reducing the nutrient amount in the reaction tank requires a very good scheduling of inflow rate.

Lemma 4.3. *If the cell mass and the nutrient amount are at a steady state ($\dot{c}_1 = 0$, $\dot{c}_2 = 0$), and if $f \neq 0$ then $g - \frac{c_2}{c_1} = 0$ holds true due to (13). As opposed to the steady state requirements of Lemmas 4.1 and 4.2, this result enables the designer to manipulate the cell mass within some limits with nonzero inflow rates.*

The same conclusion can also be drawn from the open loop system equations in (1) and (2), and the proof is straightforward.

Theorem 4.1. *Let $\dot{r}=0,\ r\neq 0$ and t_h be the hitting time, and (4) be the closed loop control law. At $t=t_h$, the system enters the steady state and for $t\geqslant t_h$, the nutrient amount is characterized by*

$$c_2(t)=\frac{c_2(0)}{c_1(0)}c_1(t)e^{I(t_h)}\qquad t\geqslant t_h \tag{21}$$

Proof. Since $g=\frac{c_2}{c_1}$ in the steady state, the transient phase is the interval $0\leqslant t\leqslant t_h$, during which the nutrient amount is characterized completely by (15). At $t=t_h$, $s(t_h)=0$ and $\dot{s}(t_h)=0$, i.e. $c_1(t_h)=r$ and $\dot{c}_1(t_h)=0$ as $\dot{r}=0$. This means that the system is in the steady state and $I(t)=I(t_h)$ for $t\geqslant t_h$ and (21) holds true. ■

Theorem 4.2. *For all steady state values maintained with $w\neq 0$, the nutrient amount is bounded and the inequality*

$$r<c_2\leqslant 2r\leqslant\frac{1+\beta}{2} \tag{22}$$

is satisfied.

Proof. Analyzing the value of $c_2(t_h)$ by utilizing $g=\frac{c_2}{c_1}$ and $c_1(t_h)=r$ at the hitting time gives

$$c_2(t_h)=\frac{(1+\beta)\mp\sqrt{(1+\beta)^2-4(1+\beta)r}}{2} \tag{23}$$

In order to have a real solution to (23), $r\leqslant\frac{1+\beta}{4}$ must be satisfied for $\forall t\geqslant t_h$ (see [12]). Considering the constraint $0\leqslant c_2\leqslant 1$, we have

$$c_2(t_h)=\frac{(1+\beta)-\sqrt{(1+\beta)^2-4(1+\beta)r}}{2} \tag{24}$$

Solving $I(t)$ from (15) lets us have

$$I(t)=\ln\frac{c_2(t)/c_1(t)}{c_2(0)/c_1(0)} \tag{25}$$

The result of Theorem 4.1 implies that for $t\geqslant t_h$

$$I(t)=I(t_h)=\ln\frac{c_2(t_h)/c_1(t_h)}{c_2(0)/c_1(0)}=\ln\frac{c_2(t_h)/r}{c_2(0)/c_1(0)} \tag{26}$$

Substituting (24) into (26) and performing appropriate rearrangements yield

$$\begin{aligned}I(t)&=\ln\left(\frac{c_1(0)}{c_2(0)}\cdot\frac{(1+\beta)-\sqrt{(1+\beta)^2-4(1+\beta)r}}{2r}\right)\\&=\ln\left(2\frac{c_1(0)}{c_2(0)}\cdot\frac{1-\sqrt{1-\theta}}{\theta}\right)t\geqslant t_h\end{aligned} \tag{27}$$

Here $\theta=\frac{4r}{1+\beta}$. Clearly, we have $0<\theta\leqslant 1$ due to the condition $r\leqslant\frac{1+\beta}{4}$, and for these values of θ, we end up with $\frac{1}{2}<\frac{1-\sqrt{1-\theta}}{\theta}\leqslant 1$. This fact with the result in (27) lets us write the inequality

$$\ln\left(\frac{c_1(0)}{c_2(0)}\right)<I(t)\leqslant\ln\left(2\frac{c_1(0)}{c_2(0)}\right)\qquad t\geqslant t_h \tag{28}$$

Utilizing the result in (21), and remembering $t\geqslant t_h$ stipulate

$$c_1(t)=r<c_2(t)\leqslant 2c_1(t)=2r \tag{29}$$

The result above and the requirement $r\leqslant\frac{1+\beta}{4}$ for obtaining nonnegative discriminant in (23) prove the theorem. ■

4.2. The Second Case, $\dot{r}\neq 0$

Theorem 4.3. *Let $u:=\frac{c_2}{c_1}$ be the ratio of nutrients per unit of cell mass. Let the expression given by (13), which characterizes the behavior of the nutrient amount, is paraphrased as*

$$\dot{u}=(g-u)(1-c_2)e^{\frac{c_2}{\gamma}} \tag{30}$$

For every possible value of the nutrient amount (c_2) satisfying $0\leqslant c_2<1$, the equilibrium value of (30) is a global attractor within Ω and the equilibrium is reached only when $u=g$ holds true.

Proof. Recall that the expression $(1-c_2)e^{\frac{c_2}{\gamma}}$ was termed w_{ss}, the steady state control action. Rewriting (30) as $\dot{u}=-w_{ss}u+w_{ss}g$ shows that u is forced to follow g as long as $0\leqslant c_2<1$ holds true. This conclusion is due to the nonnegativeness of w_{ss}. If $c_2=1$ for some time, then $w_{ss}=0$ and $\dot{u}=0$, i.e. no change in u occurs as long as $c_2=1$ is satisfied. But any nonzero inflow rate causes $0\leqslant c_2<1$, the condition of the theorem is satisfied, and u settles down to a value determined by $u=g$. The latter part of this conclusion is due to Lemma 4.2. ■

In Fig. 6, several values of $\dot{u}$ are contoured over a vector field. For every value of c_2, the illustrated vector field indicates that u tends to converge to a constant value on the thick contour labeled 0 in the figure. This curve describes the steady state $\dot{u}=(g-u)(1-c_2)e^{\frac{c_2}{\gamma}}=0$, and is a global attractor within Ω. We visualize the behavior for $0\leqslant u\leqslant 15$ for better illustration. Due to the smoothness of the involved expressions, the same behavior is seen for large values of u too.

This analysis shows that $g=u$ is forced in the closed loop, i.e. c_2 evolves bounded under the control law in (4) and its value is determined by the value of the cell mass as $u=\frac{c_2}{c_1}$. It should also be emphasized that since (13) is the general expression for the evolution of nutrient amount in the closed loop, the graphical analysis based on (30) accounts for the first case ($\dot{r}=0$) too. Clearly the control law in (4) forces the steady state ($\dot{u}=0$) described by $u=g$ for $\dot{r}\neq 0$ and the results of Theorem 4.2 hold true. When considered with the results in Fig. 6, the steady state behavior requires $1<u\leqslant 2$, which corresponds to the lower left part of the $\dot{u}=0$ curve in Fig. 6.

In the derivations presented so far, we have assumed that when the sliding mode starts, $s=0$ and $\dot{s}=0$. Furthermore, the nominal function $f(c_1,c_2)$ is assumed to be available. Yet in the application domain, it is hard to encounter these idealized conditions. Practically, due to the infinite gain when $s=0$, unnecessarily fast switching control signals are produced and very small variations in s can cause this phenomenon, which is highly undesired. This is called chattering and is a prime drawback of sliding mode control systems. Significant number of research studies addressed to obtain chattering free sliding control, and it is pointed out that switching delays and actuator dynamics do not allow the infinite frequency switching and a natural consequence is the chattering. Though not exact yet a practical remedy is to introduce a boundary layer using a function that is smooth around $s=0$ instead of the sign function (see [28,6] and the references therein). Among other alternatives, in this study, we adopt the following function with $\delta>0$ for smoothing the switching element.

$$\operatorname{sgn}(s)\approx\frac{s}{|s|+\delta} \tag{31}$$

The function in (31) resembles the original sign function as δ gets closer to zero. Conversely, the discontinuity of the sign function is changed into a very smooth transition as δ gets larger.

The design presented so far assumes that the terms seen in (1) and (2) are available for designing a controller. Although under

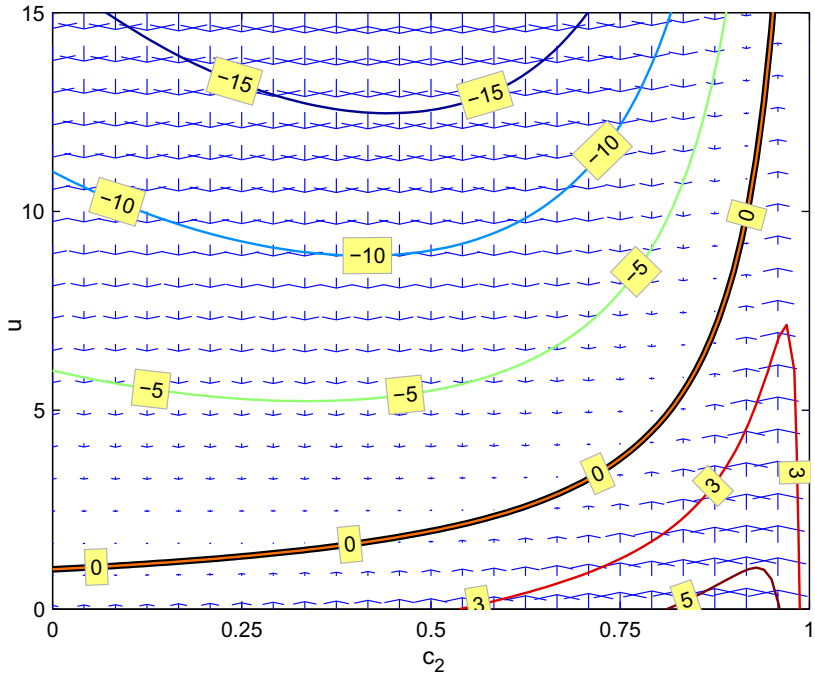

Fig. 6. Qualitative behavior of u versus c_2.

certain circumstances one may follow online estimation techniques [11], clearly, this constitutes a difficulty to alleviate as it requires knowing the structural form of the nonlinear expression under interest. This paper assumes the presence of limited amount of numerical information, which is highly practical, and exploits them to implement the proposed controller. The motivation for utilizing SVM structure for function approximation is mainly because of its ability to approach precisely mostly based on limited number of data pairs. In the next section, we summarize the SVM based function approximation scheme adopted in constructing the control law in (4). The function f is substituted by $\hat{f}$, where few data to describe f are available and $|f-\hat{f}|$ is desired to be small.

5. A Support Vector Machine (SVM) for approximating $f(c_1, c_2)$

The relevance of the SVMs to the problem in hand lies in the fact that SVMs have very powerful mapping capabilities even when the number of training data is very few. Clearly the value of such an approach becomes visible when the cost of collecting data to describe the dynamics is high. The very role of using such a mechanism is to increase the implementability of a feedback controller for a system displaying several forms of uncertainties. Since the process monitoring is an integral part of the control of such systems, typical problem formulation allows the designer to have some data instead of the functional forms. A more difficult case is when the number of data is limited. This work aims at showing the usefulness of SVMs in such cases as detailed below.

Define $\mathbf{c} = (c_1, c_2)$ and consider the regression problem over the set of pairs

$$\mathscr{D} = \{(\mathbf{c}_1, d_1), \ldots, (\mathbf{c}_N, d_N)\}, \qquad \mathbf{c}_i \in [0, 0.4] \times [0, 1], \quad d_i \in \mathbb{R} \tag{32}$$

with a function

$$\hat{f}(\mathbf{c}) = \langle \mathbf{w}, \mathbf{c} \rangle + b \tag{33}$$

where $\mathbf{w}$ and b denote the weight vector and the bias value, respectively. $\langle \cdot, \cdot \rangle$ stands for an appropriately defined operator, which is an inner product for linear regression and a kernel for nonlinear regression. Defining an $\varepsilon-$ insensitive loss function as in (34) the pairwise contribution of the ith pair is quantified.

$$L(d_i, \hat{f}(\mathbf{c}_i)) = \begin{cases} 0 & \text{if } |d_i - \hat{f}(\mathbf{c}_i)| < \varepsilon \\ |d_i - \hat{f}(\mathbf{c}_i)| - \varepsilon & \text{otherwise} \end{cases} \tag{34}$$

Clearly the $\mathbf{c}_i$s satisfying $|d_i - \hat{f}(\mathbf{c}_i)| < \varepsilon$ do not contribute the loss function and this explains how the trained SVM becomes insensitive to samples that are in the ε vicinity of the target values. Minimizing the empirical risk given by (35) lets us obtain the best values of $\mathbf{w}_i$s causing least complexity represented by $\|\mathbf{w}\|^2$;

$$R = \frac{1}{2}\|\mathbf{w}\|^2 + C\sum_{i=1}^{N} L(d_i, \hat{f}(\mathbf{c}_i)), \tag{35}$$

where C is a parameter determining the relative importance of the terms contributing to R [13]. The primal form of the optimization problem can be expressed compactly as

$$\min_{\mathbf{w},b} \quad \frac{1}{2}\|\mathbf{w}\|^2 + C\sum_{i=1}^{N}(\xi_i + \xi_i^*) \tag{36}$$

$$\text{s.t.} \quad \begin{cases} \hat{f}(\mathbf{c}_j) - d_j - \varepsilon \leqslant \xi_j, \\ d_j - \hat{f}(\mathbf{c}_j) - \varepsilon \leqslant \xi_j^*, , j = 1, 2, \ldots, N \\ \xi_j, \xi_j^* \geqslant 0, \end{cases} \tag{37}$$

where ξ_j and ξ_j^* are slack variables penalizing the deviations from the target output. The above described problem can be converted into a convex quadratic optimization problem by writing the dual representation, which is obtained after the application of Karush–Kuhn–Tucker conditions (see [13] for details). The solution can be obtained by introducing the Lagrange multipliers and performing the following minimization for $\lambda, \lambda^* \in \mathbb{R}^N$;

$$\bar{\lambda}, \bar{\lambda}^* = \arg\min_{\lambda, \lambda^*} \frac{1}{2}\sum_{i=1}^{N}\sum_{j=1}^{N}(\lambda_i - \lambda_i^*)\left(\lambda_j - \lambda_j^*\right)\langle \mathbf{c}_i, \mathbf{c}_j \rangle - \sum_{i=1}^{N}(\lambda_i - \lambda_i^*)d_i + \sum_{i=1}^{N}(\lambda_i + \lambda_i^*)\varepsilon, \tag{38}$$

with constraints $\sum_{i=1}^{N}(\lambda_i-\lambda_i^*)=0$ and $0\leqslant\lambda_i,\lambda_i^*\leqslant C$ for $i=1,2,\ldots,N$. It should be noted that the support vectors are the $\mathbf{c}_i$s for which the corresponding $\lambda_i-\lambda_i^*$ value satisfies $\varepsilon<\lambda_i-\lambda_i^*<C-\varepsilon$. Defining $\mathscr{C}$ as the set of support vectors and M as the number of elements in $\mathscr{C}$, the result of the minimization lets us obtain

$$\mathbf{w}^*=\sum_{i=1}^{N}(\lambda_i-\lambda_i^*)\mathbf{c}_i, \tag{39}$$

$$b^*=\frac{1}{M}\sum_{i=1,\ i\in\mathscr{C}}^{N}(d_i-\varepsilon\ \mathrm{sgn}(\lambda_i-\lambda_i^*)-\sum_{j=1,\ j\notin\mathscr{C}}^{N}\langle\mathbf{c}_i,\mathbf{c}_j\rangle(\lambda_j-\lambda_j^*)) \tag{40}$$

which are to be used in (33). The nonlinear regression problem is to replace the operator $\langle\cdot,\cdot\rangle$ in (32) with a kernel function satisfying the Mercer conditions (see [13,10] for details).

The rationale behind choosing ε-insensitive SVM structure for approximating the nominal function f is the following: The nominal function f should be extracted from the sparsely distributed samples, but in performing this, the SVM approximator must not memorize the map described by such a limited number of pairs. One good way is to reserve a tolerable margin for the errors in nominal plant nonlinearity through the use of a dead ε band in the cost expression. This further enables the elimination of geometrically very close data pairs that might enter the training set, which will be shown in the following section.

6. Operating conditions, results and discussion

According to the procedure and tools introduced, the control law in (4) is realized under the following operating conditions.

- As mentioned earlier, since the nominal system dynamics is known, the function $\hat{f}$ is constructed by utilizing a very limited number of numerical values. This is especially important as in real-time applications, one generally do not have access to the functional details of the system in hand. Due to powerful regression capabilities based on numerical observations, the use of SVM is a remedy among other alternatives such as fuzzy logic, neural networks or genetic algorithms, which generally suffer from the presence of multiple local minima, structure (hidden layer number or node/rule number) selection problem and overfitting [37]. Based on this, the control law in (4) is constructed by the use of $\hat{f}$ provided by the SVM module. That is to say, during the tests, we have the following control law.

$$w(t)=\frac{-\dot{r}(t)+\hat{f}(c_1,c_2)-\zeta\mathrm{sgn}(s(t))-\eta s(t)}{c_1(t)} \tag{41}$$

- The observations for the state variables $c_1(t)$ and $c_2(t)$ are noisy. The Gaussian noise sequences corrupting the state variables lie within the interval $[-0.001, 0.001]$ with a probability very close to unity. Such values for noise sequences indicate an average of -50 dB signal-to-noise ratio (SNR). The noise in the observations is a difficulty introducing uncertainties that necessitates the design of a robust controller.
- Ungar [32] emphasizes that small variations in the values of γ and β lead to significant deviations from the target cell mass. For example, given perfect measurements, 2% change in γ and 20% change in β may cause 50% deviation in the cell mass, $c_1(t)$ (see [5,32]). In this paper, we consider the nominal values of these parameters for the design of the controller and in the justification of the proposed scheme, we study these parameters with some variation in time. The necessity for investigating the behavior under parameter variations is tightly relevant to the need of exploring the controller performance under extreme conditions. In the top subplot of Fig. 7, $\gamma(t)$ is illustrated for the first 200 s of the simulation. The value of this variable changes within the interval $[0.4568, 0.5032]$, which means maximum 4.83% change in the nutrient inhibition parameter (γ). Likewise, the bottom subplot of Fig. 7 depicts the change of growth rate parameter, β. This parameter is depicted for the first 20 s of the simulation and it displays a variation in $[0.1276, 3.5717]\times 10^{-2}$ indicating a maximum of 93.62% deviation from the nominal value given by $\beta=0.02$. Clearly the chosen profiles for the variables and the presence of measurement noise entail certain degrees of robustness to meet the stability and performance requirements.

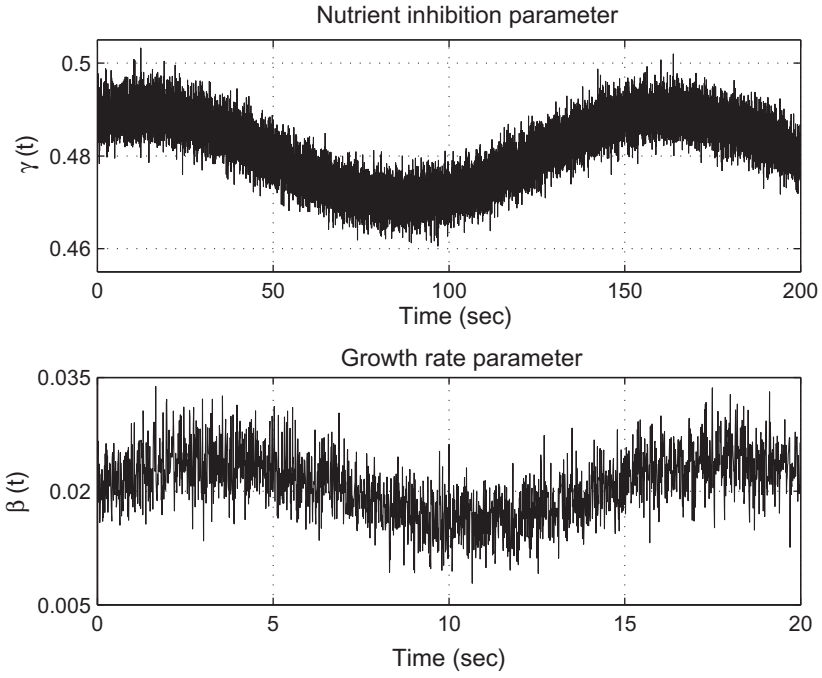

Fig. 7. The evolution of nutrient inhibition parameter (γ) and growth rate parameter (β).

- Another difficulty is the large initial errors in the cell mass. If the initial value of e_1 is large, then the controller must force it towards zero with a sequence of admissible inflow rates, $w(t)$, and must maintain the stability during the transient phase. This paper also addresses the issue of handling the large initial errors.
- The choice of the reference signal is another important issue in closed loop control. As shown in the top subplot of Fig. 8, the desired cell mass (dashed curve) claims the management of three different regimes, namely the simulation is started with a trapezoidal profile, continued with a sinusoidal profile and finally we choose a discontinuous desired profile to see how the controller stabilize the system. Although the design presented entails $\dot{r} < \infty$, i.e. differentiable reference signals, choosing this sort of a command profile enables us to figure out the qualitative and quantitative observations arise during the reaching phase especially at different cell mass ($c_1(t)$) levels.
- Next, the effect of actuation interval for the controller will be emphasized. In [32], Ungar defines $T = 50\Delta = 0.5$ s as the control interval. In other words, the inflow rate maintains its value during $nT \leqslant t < (n+1)T$, where n is a discrete time index. Consequently, the computation of the control signal applied during this interval is based on the observations at $t = nT$. The practical drawback of such an actuation scheme is the following: As discussed in the Section 2 and shown in Fig. 2, the system may get trapped to a limit cycle or an attractor during this time, or it may develop instabilities, and these make it necessary to implement a perfect flow rate management strategy. In Fig. 9, several trajectories of the controlled system are shown. The ideal control law in (4) is utilized and the nominal plant is simulated. No noise and no parametric uncertainties are considered in the figure and reference signal is $r(t) = 0.12 - 0.1\sin(\frac{2\pi t}{100})$. Clearly if there is fast control actuation, the system is suppressed to develop instabilities yet as the control period is increased, the trajectories are more likely to display deviations.
- Monitoring of process parameters, state variables, performance metrics and time variation of process subfunctions is a core component in process engineering industry. As it is the crux of the presented approach, collecting data and developing models for the real processes is an important issue in data based identification techniques. Despite their usefulness in providing data continuously, the monitoring systems contain costly hardware and software. Here, we assume that the process is not equipped with such a costly monitoring periphery yet few data from the process is achievable by experiments or from process operators. Since every chemical process has its own dynamical properties, data collection scheme becomes peculiar to each case individually. The case studied in this paper assumes few data are provided to the control system engineer.

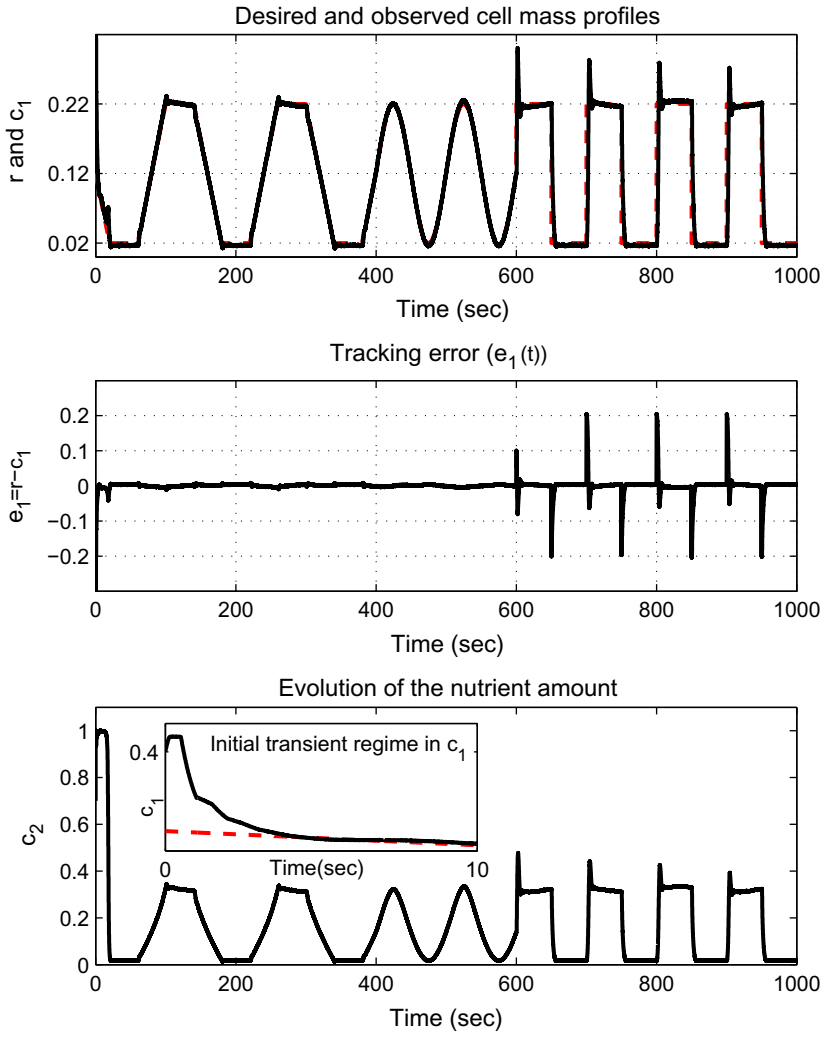

Fig. 8. The evolution of the cell mass and the nutrient amount for a given desired profile are illustrated with the tracking error and the initial transient regime.

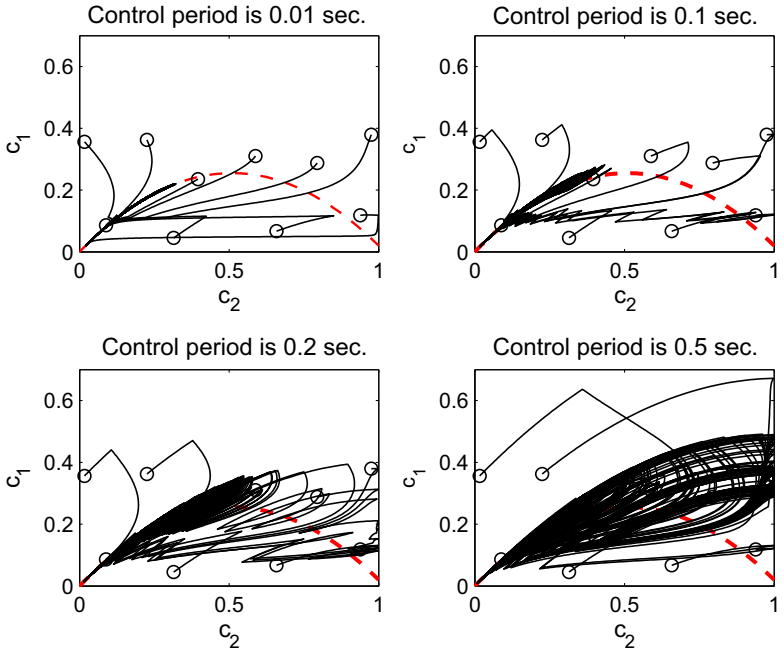

Fig. 9. Evolution of randomly initialized trajectories in the state space with ideal control law in (4). On the dashed curve $g = \frac{c_2}{c_1}$ is satisfied. Maximum value of the hitting time for trajectories seen is 1.56 s (top left), 1.91 s (top right), 2.40 s (bottom left) and 3.26 s (bottom right).

- Finally, the discrete time formulation needs emphasis. Let k denote the discrete time index. If the switching variable is chosen as $s(k) := r(k) - c_1(k)$ and discretizing the reaching law in (8) with period T would give $s(k+1) = (1-\eta\Delta)s(k) - \zeta\Delta\mathrm{sgn}(s(k))$. On the other hand, the first order Euler approximation to the derivative would let us have the discrete time representation below.

$$\begin{aligned} c_1(k+1) &= c_1(k) + \Delta(-c_1(k)w(k) + f(c_1(k), c_2(k))) \\ c_2(k+1) &= c_2(k) + \Delta(-c_2(k)w(k) + f(c_1(k), c_2(k))g(c_2(k))) \end{aligned} \tag{42}$$

Choosing

$$w(k) = \frac{-r(k+1) + c_1(k) + \Delta\hat{f}(c_1(k), c_2(k)) + (1-\eta\Delta)s(k) - \zeta\Delta\mathrm{sgn}(s(k))}{\Delta c_1(k)} \tag{43}$$

would force the stability condition $(s(k+1) - s(k))s(k) \approx -(\eta+\zeta)\Delta s(k)^2 < 0$ iff $\hat{f}(\cdot,\cdot) \approx f(\cdot,\cdot)$, and the same set of results would be obtained as the discrete time approach would consider only the integer multiples of the sampling period T.

The above issues describing the operating conditions emphasize the associated challenges of the control problem. From an industry practitioner's point of view, some of these issues may be of limited value, yet, considering them is informative in the sense of capabilities of the proposed control technique. Choice of reference signal in Fig. 8 or the time variations in the process parameters can be considered differently in a practical application yet our goal is to unfold the performance of the closed loop control system under stringent operating conditions and demanding performance expectations.

In the simulations, we have used only 30 training patterns for the training of SVM and obtained an approximate form of $\hat{f}$. The nominal function f is used in generating the training pairs and the nominal values of γ and β are utilized whenever required. The samples have been chosen randomly from the interval $(c_1, c_2) \in [0, 0.4] \times [0, 1]$ and quadratic optimization tools of Matlab® have been used in solving the optimization problem in (38). The parameters used during the optimization are, $C = 10{,}000$, $\varepsilon = 0.0001$ with a Radial Basis Function (RBF) kernel $\langle \mathbf{c}_i, \mathbf{c}_j \rangle = e^{-\frac{1}{2}\|\mathbf{c}_i - \mathbf{c}_j\|^2}$. The reason that lies behind the choices of these values is to allow very little degrees of freedom in the ε neighborhood to learn f with smallest possible number of support vectors (small but nonzero ε) but not to memorize the pairs (large but finite C) while meeting a reasonably small $\|\mathbf{w}\|^2$ value. The optimization procedure terminates at the optimum point yielding $\|\mathbf{w}\|^2 = 368.25$ and $\sum_{i=1}^{N}(\lambda_i - \lambda_i^*) = -4.1$ with 28 support vectors. Clearly, for the chosen value of ε, 2 patterns in the training set do not contribute to the loss in (34) and these patterns are not contained in the SVM basis. It is possible to utilize kernels other than RBF kernel and loss functions different from the one used here. For a list and derivation of other alternatives that can be incorporated into the design, the reader is referred to [13,10].

Now we use the approximate provided by SVM, exploit the law in (41), and perform the simulations. The other parameters of the controller are $\zeta = 0.04$, $\eta = 0.2$ and $\delta = 0.05$, which have been set after few trials. As shown in the top subplot of Fig. 8, the cell mass (solid curve) closely follows the desired cell mass profile (dashed curve). The middle subplot depicts the discrepancy between these two quantities, i.e. $e_1(t)$, or in other words, the value of the switching function, $s(t)$. The results seen emphasize that very small tracking error is maintained. The bottom subplot of the figure depicts the evolution of nutrient amount, $c_2(t)$. The variable evolves bounded as claimed in the derivation of the controller. The initial transient regime in the cell mass is illustrated in a window at the bottom of the figure, where it is convincingly apparent that hitting occurs around $t_h = 4.4$ s satisfying $t_h \leqslant \frac{|s(0)|}{\zeta} \approx 7.007$ s since $s(0) = -0.2803$.

A substantially important measure for practical applicability is the cost of physical realizability of the signals produced by the controller. The time evolution of the inflow rate corresponding to the emergence of the behavior shown in Fig. 8 is illustrated in Fig. 10. Clearly the signal is smooth enough to realize as shown also in the window plots. The top window in the figure displays the initial transient regime, whereas the bottom window depicts the

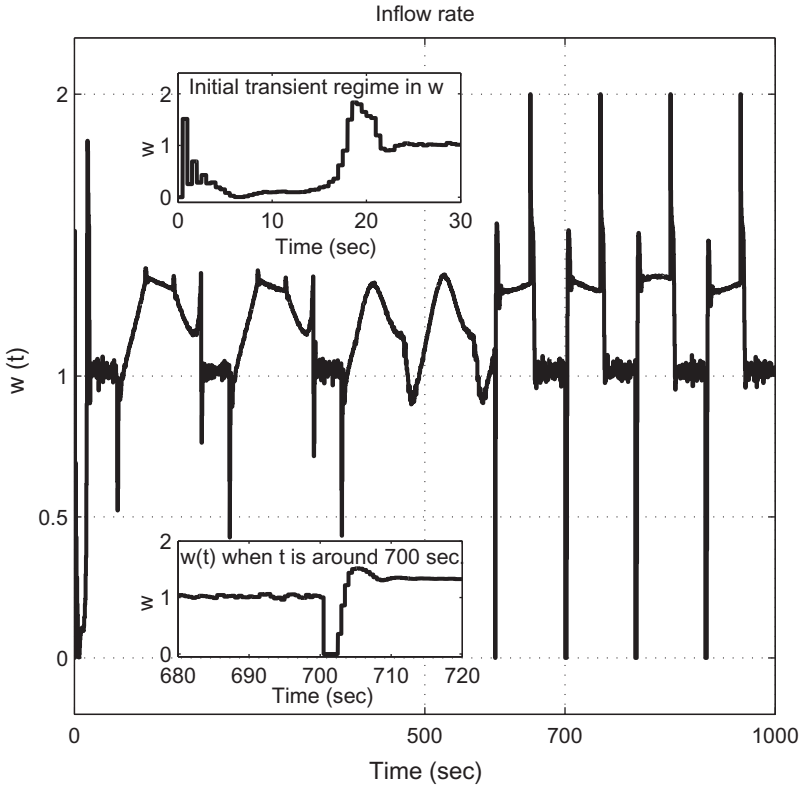

Fig. 10. The inflow rate generated by the proposed sliding mode controller.

fluctuations around $t \approx 700$ s. It is worthwhile to stress that the control signal is saturated for a very short while only when there are step changes in the command signal, i.e. the condition $\dot{r} < \infty$ is violated. During the rest of the operation, the control signal is smooth enough and the fluctuations are convergent. It is seen from Figs. 8 and 10 that the plant response has deviations around a constant value in spite of no change in the command signal. This unsteadiness in response to a steady command signal is due to the low frequency changes in the plant parameters. The effect of high frequency fluctuations is not distinguishable from the figures. These prominent features of the control signal demonstrate that the controller possesses highly desirable characteristics such as good disturbance rejection capability and guaranteed tracking precision under the presence of uncertainties. The use of (31) introduces a thin boundary layer whose thickness is determined by δ. If $s(t)$ is within the boundary layer, then it approaches the origin smoothly. This modification of the original control law gives a very slight rise to the value of t_h, which is found to be acceptable. From a practical point of view, smoothness of the control signal makes it possible to implement the control law with hardware having no or little extraordinary properties at the cost of giving very slight concessions from the performance.

Another quantity to monitor is given by $g - \frac{c_2}{c_1}$, which is forced to zero when $\dot{r} = 0$. When $\dot{r} \neq 0$, this quantity determines the evolution characteristics of c_2. Referring to Fig. 6, we have shown that the control law in (4) forces all trajectories shown in Fig. 6 to the locus described by $g - \frac{c_2}{c_1} = 0$, which explains the results shown in Fig. 12. The window plot in the figure depicts the initial transient regime, which very quickly converges to zero and the motion thereafter takes place in the vicinity of zero, i.e. $g - \frac{c_2}{c_1} \approx 0$ is maintained.

In Fig. 11, the trajectories followed in the state space are illustrated and the same initial conditions considered in Fig. 9 are selected. The trajectories are obtained with the control law in (41) and the uncertainties in the parameters β and γ are effective. The SVM provides the estimate $\hat{f}$, the observed states are noisy and the reference signal is the one shown on the top subplot of Fig. 8. Clearly, a comparison with the trajectories seen in Fig. 9 stipulates that the proposed control scheme is able to force the cell mass towards its desired value while keeping the amount of nutrients around the loci $g = \frac{c_2}{c_1}$. The system successfully alleviates the adverse effects of increasing control periods which indicate the robustness and real-time practicability of the approach.

One might wonder what happens if other values for ζ are used. According to the tests we have carried out, larger values of ζ provoke oscillations in the cell mass particularly effective as the cell mass approaches the value $\frac{1+\beta}{4}$. Larger values of η degrade the tracking performance significantly too. In fact the choice of ζ is tightly dependent upon the quantity $\sup_{c_1,c_2}|f - \hat{f}|$. If the control law is rewritten in (1) with $\hat{f}$, one obtains the expression

$$\dot{s} = -\zeta\ \mathrm{sgn}(s) - \eta\ s - (f - \hat{f}) \tag{44}$$

It is straightforward to show that the sliding subspace is an attractor, i.e. $s\dot{s} < 0$, if $|f - \hat{f}| < \zeta$ holds true. In our case, the chosen value of ζ assures this condition without provoking any undesired oscillation.

Finally, tests carried out with smaller values of the macro time steps have shown that the controller performs much better as the control interval is decreased yet this would require high sampling rates and fast computing facilities entailing costly hardware in practice.

A comparison of the controller proposed in this study and the one in [12] differs significantly in terms of tracking performance. Specifically, the control law in this reference given by

$$w = \frac{\hat{f} + c_1 - r}{c_1} \tag{45}$$

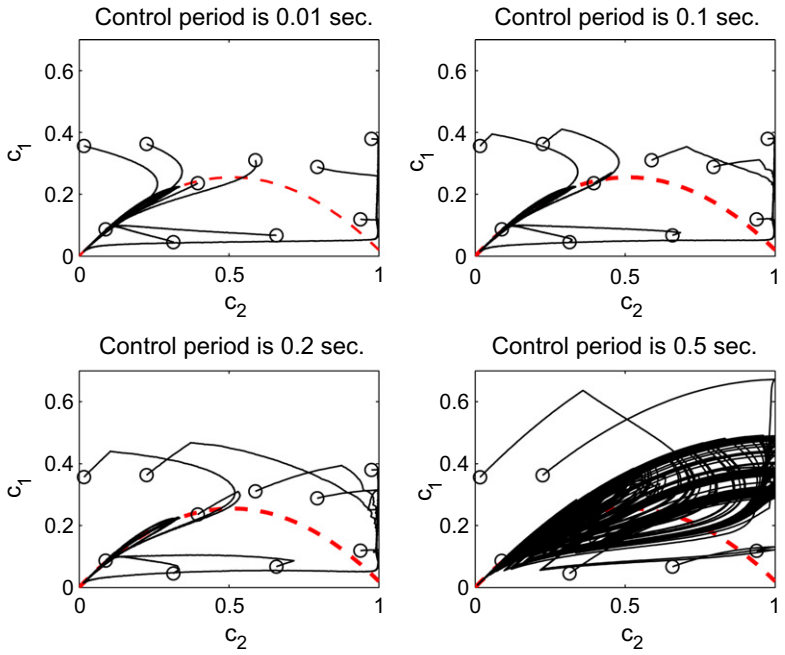

Fig. 11. Under the presence of noise and uncertainties, the evolution of randomly initialized trajectories in the state space with control law in (41). On the dashed curve $g = \frac{c_2}{c_1}$ is satisfied. Maximum value of the hitting time for the trajectories seen is 4.98 s (top left), 4.98 s (top right), 4.92 s (bottom left) and 3.26 s (bottom right).

forces $\dot{c_1} = -c_1 + r$ dynamics. Since $\hat{f} \approx c_1(1-c_2)e^{\frac{c_2}{\gamma}}$ with $\gamma = 0.48$ in (45), although the sliding mode controller maintains the tracking of the desired cell mass profile, the control law given by (45) is unable to force the plant states to their desired values. The controller fails particularly during the intervals $700 < t < 750$ s and $800 < t < 850$ s because of the variations in the nutrient inhibition parameter and the growth rate parameter. In the top left subplot of Fig. 13, the desired and the observed cell mass behaviors with the control law in (45) are depicted. Clearly the tracking precision is good till the $t = 600$ s, which is the instant when the command signal jumps from 0.12 to 0.22 suddenly. Overshoots due to step change in this subplot are visible which is also available in the response with the sliding mode controller (see Fig. 8). We denote the percent overshoot by M_p but compute it for the peaks that occur at $t = 600$ s and $t = 900$ s for the controller in (45). The results shown in this subplot together with the values tabulated in Table 1 stipulate that the sliding mode controller analyzed in this study yields considerably smaller M_p values. In other words, the capability of handling sharp

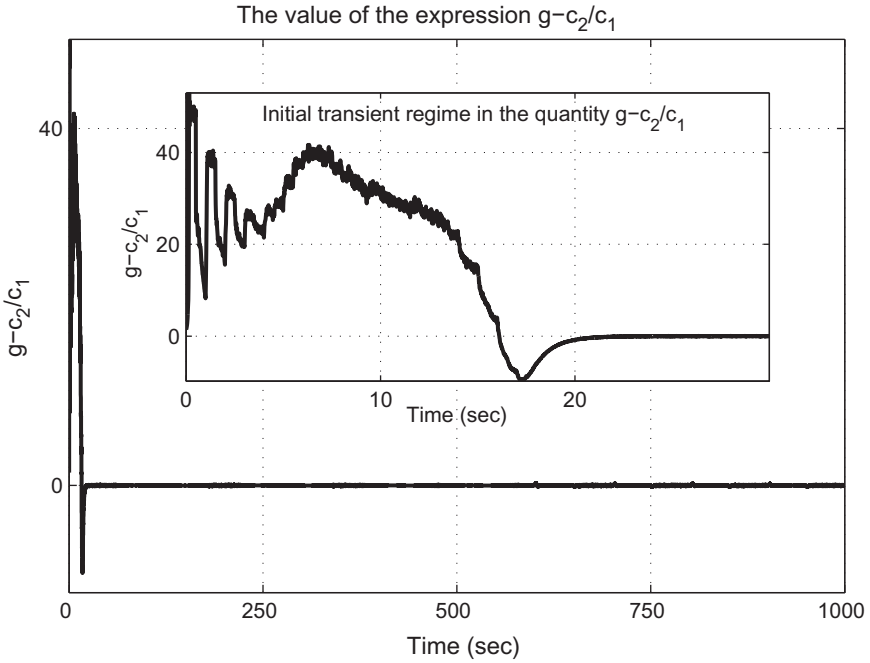

Fig. 12. The evolution of the expression $g - \frac{c_2}{c_1}$ during the course of operation.

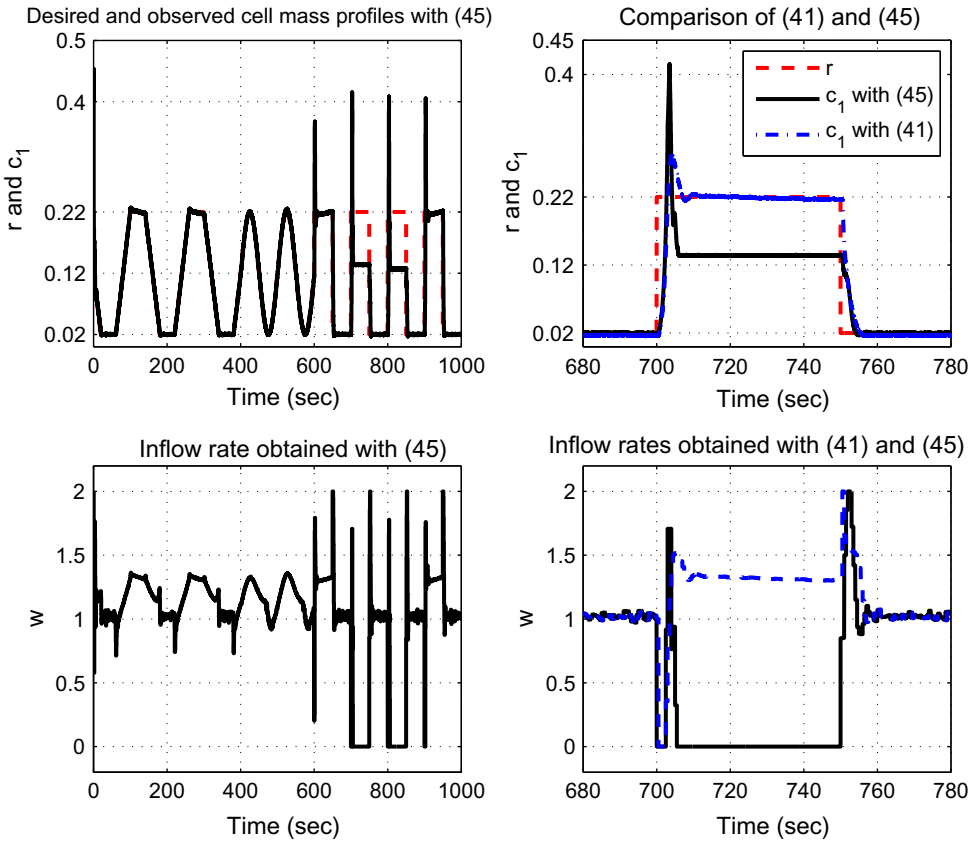

Fig. 13. A comparison of the sliding mode controller with that proposed by [12].

Table 1
A comparison of the peak values and overshoot percentages at some particular instants of time.

Time (t)	$c_1(t)$ and M_p with (41), SMC		$c_1(t)$ and M_p with (45)	
$t = 600$ s	0.300	%80.0	0.368	%148.0
$t = 700$ s	0.283	%31.5	0.415	n/a
$t = 800$ s	0.280	%30.0	0.409	n/a
$t = 900$ s	0.272	%26.0	0.401	%90.5

changes in the command signal is a prominent feature of the SVM aided sliding mode controller, and this feature is not gained through the use of the control law in (45).

In the bottom left subplot of Fig. 13, the inflow rate computed by the control law in (45) is shown. Clearly the inflow rate is zero for some periods of time and c_2 is unity. As discussed earlier in Lemma 4.2, the cell mass keeps constant below the desired value, which is an undesired result. The behavior of the cell mass during the interval $680 \leqslant t \leqslant 780$ s is depicted in the top right subplot of the figure, where the command signal is the dashed curve and the response with (41) is the dash-dotted curve, which closely follows the reference signal, and the response with (45) is the solid curve. The figure makes it possible to compare the overshoots and steady state responses clearly. Lastly in the bottom right subplot, the computed inflow rates are shown for (41) by the dash-dotted curve, (45) by the solid curve. Although the two control laws compute similar values till $t = 700$ s, after this time, the control signals and the associated responses differ dramatically.

The observations above with the facts visualized in Fig. 13 indicate that the tracking performance, robustness and disturbance rejection capability of the SVM aided sliding mode controller are remarkably better than the controller proposed in [12].

In [25], the closed loop control is achieved with neural networks and only the cell mass is assumed to be available. In that study, $\gamma = 0.416$ and $\beta = 0.016$ are used during the validation phase. These values correspond to a 5% change in γ and 20% change in β and are mentioned to degrade the performance significantly in [32]. The SVM aided sliding mode controller presented here maintains the desired cell amount with smaller amount of nutrients compared to the results in [25]. Although the only condition on c_2 is the bounded evolution, the interval for c_2 in [25] correspond to a transition in between stable and unstable regions, while the design presented here forces the system to operate at stable region only (see Fig. 5).

7. Concluding remarks

This paper considers the SVM aided semi sliding mode control of a chemical process displaying several difficulties for achieving and maintaining a satisfactory closed loop performance. The challenges associated with the plant are discussed and the derivation of the sliding mode controller are presented. The controlled variable is the cell mass within the tank and is shown to follow a desired profile while the other state variable (nutrient amount) evolves bounded. This is analyzed thoroughly and the theoretical claims are justified through simulations. It is observed that the proposed sliding mode controller displays invariance to the variations in the parameters and the noise in the measured quantities. The results obtained with the SVM aided sliding mode controller are compared with the controller proposed in [12] and it is seen that the approach presented in this study outperforms the controller in (45) in terms of tracking performance, control signal smoothness, disturbance rejection capability and robustness against uncertainties.

This paper differentiates from the existing body of literature in terms of (i) introducing an analytic explanation for the behavior of the uncontrolled state, (ii) utilizing a statistical learning theory based software tool (SVM) for constructing the control signal from sparsely distributed limited number of data, (iii) demonstrating how such a distinguishable degrees of robustness can be observed with a design based on nominal plant dynamics, (iv) providing graphical tools with physical interpretation of the conditions that are likely to occur in practice, and finally (v) postulating a fairly simple control law.

In brief, robustness is acquired through the sliding mode control law while the optimal representation in the sense of margin maximization for the plant nonlinearity is performed through an ε-insensitive SVM. The paper demonstrates the success of the cooperation of these powerful design tools on a benchmark problem with a comparison with previously published alternatives.

Acknowledgment

The comments and suggestions of the anonymous reviewers are gratefully acknowledged.

References

[1] Anderson CW, Miller III WT. Challenging control problems. In: Miller III WT, Sutton RS, Werbos PJ, editors. Neural networks for control. MIT Press; 1990. p. 475–510.
[2] Bao Z, Pi D, Sun Y. Nonlinear model predictive control based on support vector machine with multi-kernel. Chin J Chem Eng 2007;15(5):691–7.
[3] Baylar A, Batan M. Usage of artificial intelligence methods in free flowing gated closed conduits for estimation of oxygen transfer efficiency. Adv Eng Soft 2010;41(5):729–36.
[4] Bequette BW. Nonlinear control of chemical processes: a review. Ind Eng Chem Res 1991;30:1391–413.
[5] Brengel DD, Seider WD. Multistep nonlinear predictive controller. Ind Eng Chem Res 1989;28:1812–22.
[6] Camacho O, Rojas R. A general sliding mode controller for nonlinear chemical processes. Trans ASME: J Dynam Syst Measur Control 2000;122:650–5.
[7] Chen CT, Peng ST. A sliding mode control scheme for uncertain non-minimum phase CSTRs. J Chem Eng Jpn 2006;39(2):181–96.
[8] Chuang C-C, Hsu C-C, Tao CW. Embedded support vector regression on cerebellar model articulation controller with Gaussian noise. Appl Soft Comput 2011;11(1):1126–34.
[9] Colantonio MC, Desages AC, Romagnoli JA, Palazoglu A. Nonlinear control of a CSTR: disturbance rejection using sliding mode control. Ind Eng Chem Res 1995;34:2383–92.
[10] Cristianini N, Shawe-Taylor J. An introduction to support vector machines and other kernel-based learning methods. Cambridge University Press; 2000.
[11] Dochain D, Perrier M. Bioprocess control. Bioreaction engineering: modeling and control. Berlin: Springer; 2000. p. 145–66.
[12] Efe MÖ, Abadoglu E, Kaynak O. A novel analysis and design of a neural network assisted nonlinear controller for a bioreactor. Int J Robust Nonlinear Control 1999;9(11):799–815.
[13] Gunn SR. Support vector machines for classification and regression. ISIS Technical Report. United Kingdom: University of Southampton; 1998.
[14] Han L, Chen G. A fuzzy clustering method of construction of ontology-based user profiles. Adv Eng Soft 2009;40(7):535–40.
[15] Hanczyc EM, Palazoglu A. Sliding mode control of nonlinear distributed parameter chemical processes. Ind Eng Chem Res 1995;34:557–66.
[16] Hung JY, Gao W, Hung JC. Variable structure control: a survey. IEEE Trans Ind Electron 1993;40(1):2–22.
[17] Iplikci S. A support vector machine based control application to the experimental three-tank system. ISA Trans 2010;49(3):376–86.
[18] Iplikci S. Support vector machines based neuro-fuzzy control of nonlinear systems. Neurocomputing 2010;73(10–12):2097–107.
[19] Kaya I. Sliding-mode control of stable processes. Ind Eng Chem Res 2007;46(2):571–8.
[20] Kaynak O, Harashima F, Hashimoto H. Variable structure systems theory, as applied to sub-time optimal position control with an invariant trajectory. Trans Inst Elect Eng Jpn E 1984;104:4752.
[21] Khalil H. Nonlinear systems. New Jersey: Prentice Hall; 2001.
[22] Lute VA, Singh Upadhyay KK. Support vector machine based aerodynamic analysis of cable stayed bridges. Adv Eng Soft 2009;40(9):830–5.
[23] Li Z, Zhang Y, Yang Y. Support vector machine optimal control for mobile wheeled inverted pendulums with unmodelled dynamics. Neurocomputing 2010;73(13–15):2773–82.
[24] Li J, Zhang Y, Pan H. Chattering-free LS-SVM sliding mode control. Lect Notes Comput Sci: Adv Neural Networks 2008;5263:701–8.
[25] Puskorius GV, Feldkamp LA. Neurocontrol of nonlinear dynamical systems with kalman filter trained recurrent networks. IEEE Trans Neural Networks 1990;5(2):279–97.
[26] Rodil SS, Fuente MJ. Fault tolerance in the framework of support vector machines based model predictive control. Eng Appl Artificial Intell 2010;23(7):1127–39.
[27] Shin J, Kim HJ, Park S, Kim Y. Model predictive flight control using adaptive support vector regression. Neurocomputing 2010;73(4-6):1031–7.
[28] Slotine J-JE, Li W. Applied nonlinear control. New Jersey: Prentice Hall; 1991.
[29] Suykens JAK, Vandewalle J, De Moor B. Optimal control by least squares support vector machines. Neural Networks 2001;14(1):23–35.
[30] Tokat S. Time-varying sliding surface design with support vector machine based initial condition adaptation. J Vibr Control 2006;12(8):901–26.
[31] Tokat S, Iplikci S, Ulusoy L., Output feedback sliding mode control with support vector machine based observer gain adaptation. In: Proceedings of the 8th WSEAS international conference on circuits, systems, electronics, control & signal processing, Puerto De La Cruz, Tenerife, Canary Islands, Spain; 2009. pp. 63–8.
[32] Ungar LH. A bioreactor benchmark for adaptive-network based process control. In: Miller III WT, Sutton RS, Werbos PJ, editors. Neural networks for control. MIT Press; 1990. p. 387–402.
[33] Utkin VI. Sliding modes in control optimization. New York: Springer-Verlag; 1992.
[34] Vapnik V. The nature of statistical learning theory. New York: Springer-Verlag; 1995.
[35] Wang H, Pi D, Sun Y. Online SVM regression algorithm-based adaptive inverse control. Neurocomputing 2007;70(4-6):952–9.
[36] Wang Y-N, Yuan X-F. SVM approximate-based internal model control strategy. Acta Automat Sinica 2008;34(2):172–9.
[37] Wang X-D, Ye M-Y. Nonlinear dynamic system identiication using least squares support vector machine regression. In: Proceedings of the 3rd international conference on machine learning and cybernetics, Shanghai, August 26–29 2004. p. 941–5.
[38] Young KD, Özgüner Utkin VI, Ü. A control engineer's guide to sliding mode control. IEEE Trans Control Syst Technol 1999;7(3):328–42.